Collective Motion of Microorganisms in a Viscoelastic Fluid

Gaojin Li and Arezoo M. Ardekani

Phys. Rev. Lett. **117**, 118001 — Published 7 September 2016

DOI: 10.1103/PhysRevLett.117.118001

Collective motion of microorganisms in a viscoelastic fluid

Gaojin Li and Arezoo M. Ardekani*
School of Mechanical Engineering, Purdue University, West Lafayette, IN 47907, USA
(Dated: August 10, 2016)

We study the collective motion of a suspension of rod-like microswimmers in a two-dimensional film of viscoelastic fluids. We find that the fluid elasticity has a small effect on a suspension of pullers, while it significantly affects the pushers. The attraction and orientational ordering of the pushers are enhanced in viscoelastic fluids. The induced polymer stresses break down the large-scale flow structures and suppress velocity fluctuations. In addition, the energy spectra and induced mixing in the suspension of pushers are greatly modified by fluid elasticity.

The suspension of swimming microorganisms and their aggregation have received growing attention for their importance in pathology, reproduction and ecology [1]. The collective motion of microorganisms exhibits some turbulent-like features, such as large-scale flow structures [2, 3], strong fluctuations in velocity field [4], and enhanced diffusion and mixing [5]. The microorganisms exhibit locally correlated motions [6] and aggregations [2]. In contrast to the classic turbulence at high Reynolds numbers, which involves energy transfer across different length scales, the active turbulence is generated by the collective motion of microorganisms. The input energy is dissipated at the same length scale as it is produced [7, 8]. Theoretical models based on continuum equations [9] and discrete self-propelled particles [10–13] have been proposed to investigate the stability and turbulent features of microswimmer suspensions and active nematics [14].

Microorganisms and spermatozoa often swim in non-Newtonian fluids which are viscoelastic [15]. Examples of these phenomena include bacteria forming biofilms by producing extracellular polymeric substances [16], spermatozoa racing through cervical mucus in the mammalian female reproductive tract [17], and bacteria abundance within oceanic gels of transparent exopolymer particles [18]. There has been a long debate about the effects of fluid elasticity on the speed of an isolated swimmer. Both an increase and a decrease in speed have been observed in previous studies depending on the propulsion mechanism and geometry of the microorganisms and fluid's rheological properties [19]. In a dilute suspension of microorganisms, fluid elasticity changes the wavelength of the most unstable disturbance [20] and leads to microorganism aggregation in an external vortical flow [21]. More recently, a continuum model was developed [22] to couple the internally driven active nematic to the polymer rheology. The results show that the polymer additives may have a calming effects on the active flow, while the full-coupling of the polymer and nematic orientations greatly increases the complexity of spontaneous flow. At high Reynolds numbers, polymer additives in a turbulent flow suppress the large-scale fluctuations [23], increase flow intermittency [24] and generate a significant drag reduction [25]. The interplay between stretching of polymer molecules and turbulent flow structures [26] is one of the key aspects of viscoelastic turbulence.

In this letter, we present the first fully resolved numerical simulation of collective dynamics of microswimmers in viscoelastic fluids. The present work introduces fluid elasticity as a mean to tune the effective interactions between swimmers and consequently their collective motion. Different from the previous works [20, 22], we consider the hydrodynamics of the discrete rod-like swimmers in a continuum viscoelastic fluid. We show that the fluid elasticity has a stronger effect on a suspension of pushers than pullers. The polymer stress enhances the local aggregation and polar alignment of pushers. At large scales, polymers suppress the velocity fluctuations and break down the large-scale flow structures. Accordingly, energy spectra and induced mixing in a suspension of microswimmers are modified by fluid elasticity.

We conduct two-dimensional simulations of N identical slender rod-like swimmers in a viscoelastic fluid. Simulations are performed in a square box of size L with periodic boundaries in all directions. The number density is defined as $c = Nl^2/L^2$. By imposing a slip velocity $U_s = U_0[\pm \tanh(10s/l) + 1]$ on the surface of the swimmer, we consider both pushers (+) and pullers (-). Here, U_0 is the characteristic swimming speed, l is the swimmer length, $s \in [-l/2, l/2]$ is the length measured from the head of the swimmer. In a Newtonian fluid, the swimming speed of an isolated pusher and puller is $U = U_0$; their induced velocity fields are also the same but in the opposite direction. Hereinafter, the results are normalized as follows: the length is scaled by l, velocity by U_0, time by l/U_0, and pressure and stress by $\rho\nu U_0/l$, where ρ and ν are the fluid density and kinematic viscosity, respectively.

The dimensionless equations for conservation of momentum and mass are

$$Re\frac{D\boldsymbol{u}}{Dt} = -\nabla p + \nabla\cdot\boldsymbol{\tau} + \boldsymbol{f}, \qquad \nabla\cdot\boldsymbol{u} = 0, \tag{1}$$

where the Reynolds number $Re = U_0 l/\nu$ is 5×10^{-3}, D/Dt is the material time derivative, $\boldsymbol{u}$ is the velocity vector, p is the pressure and $\boldsymbol{\tau}$ is the deviatoric stress tensor. The forcing term $\boldsymbol{f}$ is calculated using a distributed Lagrange multiplier method to accurately sat-

isfy the boundary conditions on the swimmer [27] (see more details in [28]). In a Newtonian fluid, the stress tensor is $\boldsymbol{\tau} = \dot{\boldsymbol{\gamma}}$, where $\dot{\boldsymbol{\gamma}} = \nabla \boldsymbol{u} + \nabla \boldsymbol{u}^{\mathrm{T}}$ is the shear rate tensor. To model an elastic fluid, the Oldroyd-B constitutive equation is used, in which $\boldsymbol{\tau}$ can be split into solvent and polymer contributions as $\boldsymbol{\tau} = \boldsymbol{\tau}^s + \boldsymbol{\tau}^p$, where $\boldsymbol{\tau}^s = \beta_s \dot{\boldsymbol{\gamma}}$ and

$$\boldsymbol{\tau}^p + De\, \overset{\triangledown}{\boldsymbol{\tau}}^p = (1-\beta_s)(\nabla \mathbf{u} + \nabla \mathbf{u}^{\mathrm{T}}), \qquad (2)$$

where $\beta_s = 0.5$ is the ratio of the solvent viscosity to the zero-shear-rate viscosity of the polymeric solution. The Deborah number $De = \lambda / t_f$ is the ratio of the polymer relaxation time λ to the characteristic flow time scale $t_f = l/U_0$. In a viscoelastic turbulence, the flow field is strongly affected by De. At $De \ll 1$, polymer molecules are essentially not deformed and the elastic effects are negligible. In contrast, at $De \gg 1$, elastic forces dominate. The notation $\triangledown$ represents the upper-convected derivative. The excluded volume effect is modeled by adding a linear repulsive force whenever the distance between any two points on two swimmers is smaller than the swimmer thickness.

The effects of fluid elasticity on a single swimmer are first investigated. For a pusher, polymers are tangentially stretched along the entire body [Fig. 1*a*], while for a puller, the high elastic energy is stored near the tail [Fig. 1*b*]. The flow field induced by the swimmers are affected by fluid elasticity [Fig. 1*c*]. In a Newtonian fluid, the magnitude of the velocity field in front of and behind the swimmer are the same $|u| \sim 1/r$. Fluid elasticity breaks this symmetry and its effects on pushers and pullers are different. The same $1/r$ scaling law holds for pullers, while for pushers, velocity decreases more rapidly at the rear side of the swimmer. The polymer molecules are strongly stretched along the pusher, once they pass the swimmer, the polymer extension can not be supported any longer and the fluid elements contract along the swimming direction and expand in the normal direction. Therefore, streamlines expand at the rear of the swimmer, and flow velocity along the swimmer direction dramatically decreases, similar to the "die swell" phenomenon [36]. Fluid elasticity does not affect the far-field velocity decay for either swimmers since the polymers are mainly deformed near the swimmer. Fluid elasticity hinders the swimming speed for both pushers and pullers for an isolated swimmer. The average swimming speed of pushers in a suspension is larger than an isolated swimmer and monotonically decreases with De, while it is less affected for a suspension of pullers [Fig. 1*d*]. Therefore, the role of fluid elasticity on a suspension can be very different from its effects on a single swimmer.

In suspensions, the swimmers are initially uniformly distributed and have the same swimming direction. The nematic suspension is unstable for both swimmer types, and they form clusters. Fig. 2 shows the flow field at

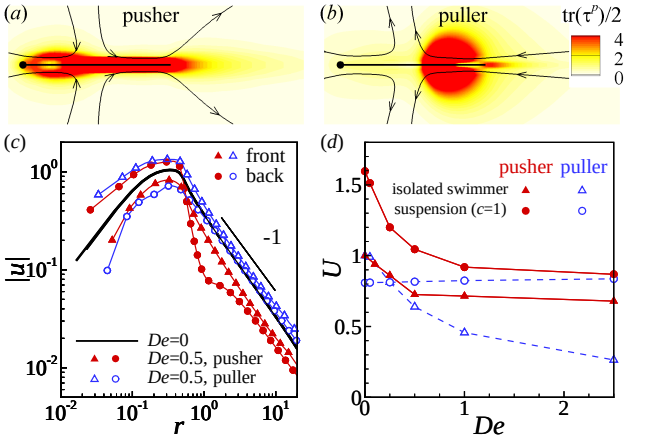

FIG. 1. (color online). Distribution of elastic energy $\mathrm{tr}(\boldsymbol{\tau}^p)/2$ around a (*a*) pusher and (*b*) puller as they swim to the left, $De = 0.5$. (*c*) The magnitude of the velocity field around an isolated swimmer. (*d*) Swimming speed for an isolated swimmer (triangles) and suspension (circles) as a function of De.

$t = 25$ which has reached a statistically steady state. In a Newtonian fluid, the flow induced by pushers is characterized by large scale structures as large as the size of computational domain. Pushers tend to align with their neighbors due to the lateral hydrodynamic attractions and they exhibit a local orientational order. The suspension of pullers in a film is very different from those in an unconfined suspension. In a bulk fluid, large scale flows are not observed and the pullers are randomly distributed regardless of their concentration [11]. Whereas in a film, the pullers aggregate at the front and form clusters [Fig. 2(*b*)].

In a viscoelastic fluid [Fig. 2(*c*) and (*d*)], the cluster type is not qualitatively affected, i.e. the aggregation of the swimmers is mainly determined by their swimming mechanism. The typical cluster size for pushers in a viscoelastic fluid is, however, larger and involves more swimmers compared to the Newtonian fluid. Fluid elasticity reduces the velocity fluctuations and suppresses the fluid mixing (see more details in [28]). Fluid elasticity reduces the size of large-scale flow structures in a suspension of pushers, which can be as large as the computational domain in a Newtonian fluid. These large-scale high-speed regions occasionally form in a viscoelastic fluid, but quickly break down into smaller patches (see movies in [28]). Fluid elasticity has much weaker effects on a suspension of pullers.

In Fig. 3(*a*), the aggregation of swimmers are quantified using pair correlation functions $g(r)$ and $g(\theta)$, representing the probability of finding a swimmer at center-to-center distance r and angle θ with respect to another swimmer. For pushers, $g(r)$ peaks at around $r = 0.2$, representing the strong tendency of lateral attraction. The

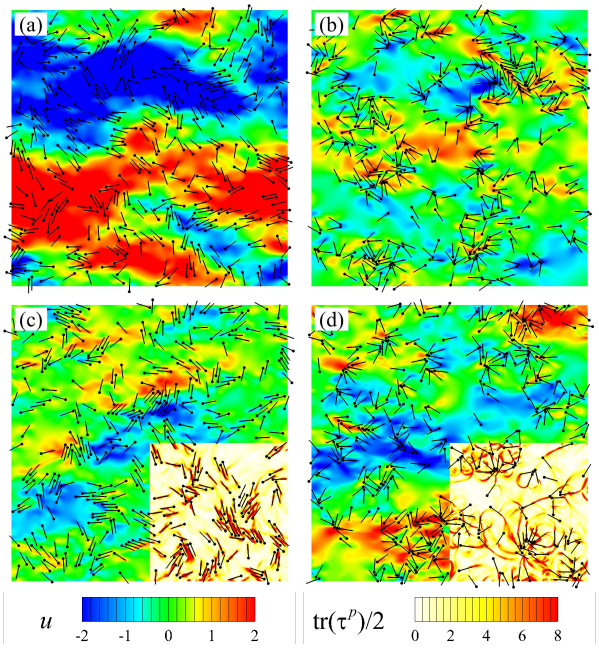

FIG. 2. (color online). Flow field and distribution of swimmers at $t = 25$ for (a, c) pushers and (b, d) pullers. The number density is $c = 1$. $De = 0$ in (a, b) and 2.5 in (c, d), respectively. Contours in the main frame and the right-bottom quarter of (c, d) show the horizontal velocity component u and elastic energy $\mathrm{tr}(\boldsymbol{\tau}^p)/2$, respectively. For movies see [28].

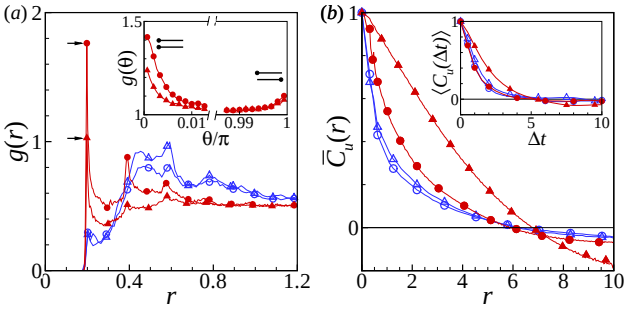

FIG. 3. (color online). (a) Pair correlation functions $g(r)$ and $g(\theta)$ (inset) for pushers (red) and pullers (blue). Contour plots of $g(r, \theta)$ are given in [28]. (b) Averaged spatial and temporal (inset) velocity correlations $\overline{C}_u(\boldsymbol{r})$ and $\langle C_u(\Delta t)\rangle$ of the induced flow field. The number density is $c = 1$. Solid triangle: pusher at $De = 0$, solid circle: pusher at $De = 2.5$, open triangle: puller at $De = 0$ and open circle: puller at $De = 2.5$.

peak value of $g(r)$ increases with De, showing an increase in attraction due to fluid elasticity. In the inset, the plot of $g(\theta)$ shows a tendency for polar alignment of pushers, and fluid elasticity further increases this effect. In general, fluid elasticity enhances the aggregation of pushers, which is consistent with our results for two hydrodynamically interacting pushers (see more details in [28]). Shear flow in the gap between the two pushers generates a strong polymer stretching which enhances the attraction. This mechanism is similar to the polymer-enhanced wall attraction of a pusher-type squirmer [37].

The role of fluid elasticity on the flow coherent structures is characterized by the spatial and temporal correlation functions as $C_u(r) = \langle \boldsymbol{u}(\boldsymbol{x}+\boldsymbol{r})\cdot\boldsymbol{u}(\boldsymbol{x})\rangle / \langle \boldsymbol{u}^2(\boldsymbol{x})\rangle$ and $C_u(\Delta t) = \overline{\boldsymbol{u}(t+\Delta t)\cdot\boldsymbol{u}(t)}/\overline{\boldsymbol{u}^2(t)}$. Here, $\langle\rangle$ and $-$ represent the average in space and time, respectively. In Fig. 3(b), we compare the averaged correlation functions $\overline{C}_u(r)$ and $\langle C_u(\Delta t)\rangle$ for different suspensions. The spatial velocity correlation for a pusher suspension is weakened by fluid elasticity. The typical length of the averaged flow structures, which is characterized by the value of r at which $\overline{C}_u(r) = 0$ only slightly decreases with De. Similarly, the shape of the temporal velocity correlation function is changed by fluid elasticity, while correlation time $\Delta t \simeq 5$ is less affected. Fluid elasticity reduces the velocity magnitude of some regions of the large-scale flow, while it is not strong enough to reverse the flow direction.

We now closely examine the instantaneous flow field to better understand the interplay between polymer stretching, swimmer aggregation and large-scale flow structures in a suspension of pushers. The time variation of the kinetic and elastic energies in a suspension is written as

$$Re\frac{dK}{dt} + \frac{dE}{dt} = P - \varepsilon_K - \varepsilon_E, \tag{3}$$

where $K = \langle \boldsymbol{u}^2/2\rangle$ and $E = \langle \mathrm{tr}(\boldsymbol{\tau}^p)/2\rangle$ are the spatial averaged kinetic and elastic energies in the flow field. $P = \sum_i \int_l \boldsymbol{f}\cdot\boldsymbol{u} ds/L^2$ is the average power input generated by all the swimmers. $\varepsilon_K = \langle \beta_s\dot{\boldsymbol{\gamma}} : \dot{\boldsymbol{\gamma}}\rangle$ and $\varepsilon_E = E/De$ represent energy dissipations caused by the Newtonian solvent and polymer molecules, respectively. To quantify the pusher aggregation, we define a local polar order parameter $S_1 = \sum_i \sum_{j\neq i, r<1} \cos(\theta)$, where r and θ are the distance and angle between pushers i and j. Parameter S_1 provides information about the polar alignment of pushers, including the size and the number of clusters. For N pushers aggregated in one cluster with perfect polar alignment, $S_1 = N(N+1)$. Similarly, we define a local nematic parameter $S_2 = \sum_i \sum_{j\neq i, r<1} |\cos(\theta)|$. The size of instantaneous flow structure r_c is determined by calculating $C_u(r_c) = 0$. At $De = 0$, $\overline{K} \simeq 1.8, \overline{S}_1 = 113.5, \overline{S}_2 = 1048.2$ and $\overline{r}_c \simeq 6.6$; at $De = 2.5$, $\overline{K} \simeq 0.4, \overline{S}_1 = 260.9, \overline{S}_2 = 1238.2, \overline{r}_c \simeq 5.9$, and $\overline{E} \simeq 2.6$. Fluid elasticity reduces velocity fluctuations, enhances polar and nematic alignment of pushers, and slightly decreases the size of the average large-scale flow structures.

To better understand the results, we compare fluctuations for different variables, $a' = (a - \overline{a})/\overline{a}$, where a is the variable of interest. In Fig. 4(a), K' and r_c' are strongly correlated in a Newtonian fluid, meaning larger flow structures generate stronger velocity fluctua-

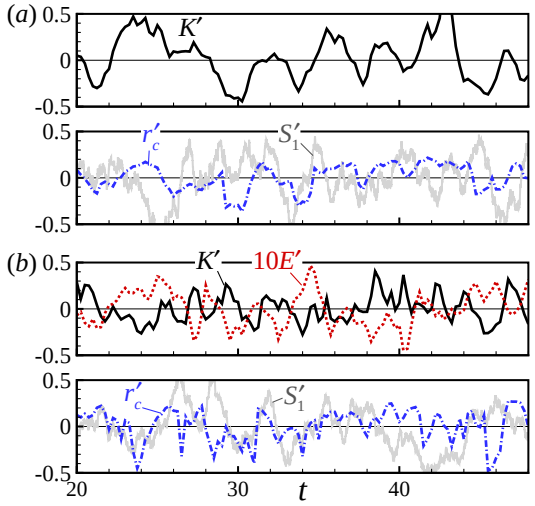

FIG. 4. (color online). The fluctuation of the normalized kinetic energy K' (solid black line) correlates with the flow structure size r'_c (dashdot blue line) in a pusher suspension at $c = 1$ in both (a) Newtonian and (b) viscoelastic ($De = 2.5$) fluids, while there is no obvious correlation with the local polar order parameter S_1. The elastic energy E' (dashed red line) is anti-correlated with K' in a viscoelastic fluid.

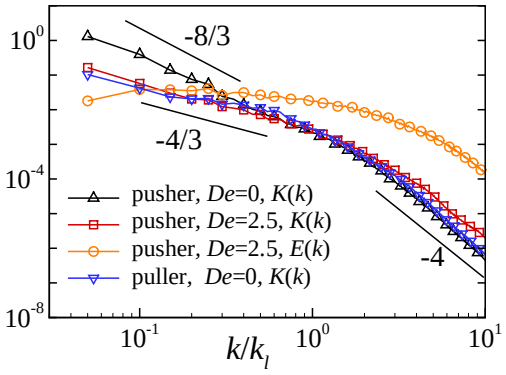

FIG. 5. (color online). Energy spectra $K(k)$ and $E(k)$ in a microswimmer suspension at $c = 1$. Fluid elasticity reduces the slope of the kinetic energy spectrum at $k < k_l$ in a pusher suspension.

tions. No obvious correlation between S'_1 and r'_c is observed, indicating that the pusher aggregation is more related to the local hydrodynamic interaction among the swimmers, rather than large-scale flows. Both K' and r'_c oscillate with a typical time period $\Delta t \sim 4$, which is approximately the time it takes for a pusher to swim across large-scale flow structures. In Fig. 4(b), K' and E' are anti-correlated with each other in a viscoelastic fluid. Note that because of the Re factor in Eq. (3), the elastic energy strongly affects the kinetic energy, even though E' is an order of magnitude smaller than K'. The time scale of fluctuations is approximately $\Delta t = 1 \sim 2$, which is close to the polymer relaxation time $\lambda = 2.5$. Polymer stretching in the suspension of microswimmers is a highly nonequilibrium process. Once the large-scale flow emerges, it starts to more strongly stretch polymer molecules in the flow field. The polymer stretching gradually reduces the velocity fluctuations and breaks down the large-scale flow structures. After the polymer molecules are relaxed, the velocity fluctuations are recovered and large-scale flow structures emerge again.

The modification of the flow coherent structures by fluid elasticity is also revealed in energy spectra. In Fig. 5, we compare the energy spectrum for different suspensions. For all the cases, k^{-4} power-law is observed at high wavenumbers $k > k_l$, due to the shape of rod-like swimmers. At low wavenumbers, the asymptote varies with the swimmer type and the fluid environment. For a suspension of pushers in a Newtonian fluid, we derive the same scaling $K(k) \sim k^{-8/3}$ as in a bacterial suspension [7]. In a viscoelastic fluid, the kinetic energy reduces to $k^{-4/3}$ at low wavenumbers and slightly increases at high wavenumbers $k > k_l$. We speculate that polymer molecules extract energy from large scales and partially release it at small scales. In a viscoelastic turbulent flow at high Re [38], the interaction between polymer molecules and large scale flows effectively causes a polymer-induced kinetic energy cascade. We expect the same mechanism to be present in a suspension of pushers in a viscoelastic fluid, except that unlike viscoelastic turbulent flows at high Re, this is the only energy cascade. The elastic energy has a much more flat distribution over $k < k_l$, indicating the polymer stretching by the large scale flows. This is similar to the viscoelastic turbulence at high Reynolds numbers [39]. The kinetic energy dissipation is $\varepsilon_K(k) = 2k^2K(k) \sim k^{-2/3}$ for a pusher suspension in a Newtonian fluid. The viscous dissipation is mainly caused by the large-scale flow structures, consistent with the measurements in a bacterial suspension [40]. In a viscoelastic fluid, polymers add an extra dissipation ε_E to the fluid and $\varepsilon_K(k) \sim k^{2/3}$ at $k < k_l$, i.e. the strongest viscous dissipation occurs at the swimmer length scale.

To conclude, based on the fully-resolved numerical simulations of suspension of rod-like swimmers, we have shown that the effects of fluid elasticity on a suspension can be very different from its effect on a single swimmer. Particulary, fluid elasticity enhances the aggregation of pushers mainly due to the local hydrodynamics. Large-scale flow structures induce stronger polymer stretching, and the polymer relaxation breaks down the large flow structures and suppresses the velocity fluctuations. Our work has extended the studies of collective motion in Newtonian fluids to polymeric solutions. These results can be useful in understanding the behavior of swimming microorganisms in a more realistic fluid environment, such as bacteria in biofilm and oceanic exopolymer

particles.

We acknowledge the anonymous referees for constructive suggestions. This research is supported by grants from BP/The Gulf of Mexico Research Initiative and NSF CBET-1445955-CAREER.

* ardekani@purdue.edu

[1] J.W. Costerton, P.S. Stewart and E.P. Greenberg, Science **284**, 1318 (1999); I.H. Riedel, K. Kruse and J. Howard, Science **309**, 300 (2005); N. Blackburn, T. Fenchel and J. Mitchell, Science **282**, 2254 (1998).

[2] C. Dombrowski, L. Cisneros, S. Chatkaew, R.E. Goldstein and J.O. Kessler, Phys. Rev. Lett. **93**, 098103 (2004); A. Sokolov, I.S. Aranson, J.O. Kessler and R.E. Goldstein, Phys. Rev. Lett. **98**, 158102 (2007).

[3] N.H. Mendelson, A. Bourque, K. Wilkening, K.R. Anderson and J.C. Watkins, J. bacteriol. **181**, 600 (1999); A. Sokolov, I.S. Aranson, J.O. Kessler and R.E. Goldstein, Phys. Rev. Lett. **98**, 158102 (2007).

[4] L.H. Cisneros, R. Cortez, C. Dombrowski, R.E. Goldstein and J.O. Kessler, Exp. Fluids **43**, 737 (2007); Q. Liao, G. Subramanian, M.P. DeLisa, D.L. Koch and M. Wu, Exp. Fluids **19**, 061701 (2007).

[5] X.-L. Wu and A. Libchaber, Phys. Rev. Lett. **84**, 3017 (2000); A. Sokolov, R.E. Goldstein, F.I. Feldchtein and I.S. Aranson, Phys. Rev. E **80**, 031903 (2009); H. Kurtuldu, J.S. Guasto, K.A. Johnson and J.P. Gollub, Proc. Natl. Acad. Sci. U.S.A. **108**, 10391 (2011).

[6] L.H. Cisneros, J.O. Kessler, S. Ganguly and R.E. Goldstein, Phys. Rev. E **83**, 061907 (2011).

[7] H.H. Wensink, J. Dunkel, S. Heidenreich, K. Drescher, R.E. Goldstein, H. Löwen and J.M. Yeomans, Proc. Natl. Acad. Sci. U.S.A. **109**, 14308 (2012).

[8] A. Creppy, O. Praud, X. Druart, P.L. Kohnke and F. Plouraboué, Phys. Rev. E **92**, 032722 (2015).

[9] D. Saintillan and M.J. Shelley, Phys. Rev. Lett. **100**, 178103 (2008); M. Leoni and T.B. Liverpool, *ibid.* **105**, 238102 (2010); J. Dunkel, S. Heidenreich, K. Drescher, H.H. Wensink, M. Bär and R.E. Goldstein, *ibid.* **110**, 228102 (2013).

[10] R.A. Simha and S. Ramaswamy, Phys. Rev. Lett. **89**, 058101 (2002).

[11] D. Saintillan and M.J. Shelley, Phys. Rev. Lett. **99**, 058102 (2007).

[12] D. Saintillan and M.J. Shelley, J. R. Soc. Interface, 571585 (2011).

[13] D. Krishnamurthy and G. Subramanian, J. Fluid Mech., **781** 422-466 (2015).

[14] L. Giomi, Phys. Rev. X **5**, 031003 (2015).

[15] S.H. Hwang, M. Litt and W.C. Forsman, Rheol. Acta **8**, 438 (1969); I. Klapper, C.J. Rupp, R. Cargo, B. Purvedorj and P. Stoodley, Biotechnol. Bioengng **80**, 289 (2002); C. Storm, J.J. Pastore, F.C. MacKintosh, T.C. Lubensky and P.A. Janmey, Nature **435**, 7039 (2005).

[16] L. Hall-Stoodley, J.W. Costerton, and P. Stoodley, Nature Rev. Microbiol. **2**, 95 (2004).

[17] S. Suarez and A. Pacey, Hum. Reprod. update **12**, 23 (2006).

[18] D.C. Smith, M. Simon, A.L. Alldredge and F. Azam, Nature **359**, 139 (1992).

[19] E. Lauga, Phys. Fluids **19**, 083104 (2007); J. Teran, L. Fauci and M. Shelley, Phys. Rev. Lett. **104**, 038101 (2010); X.N. Shen and P.E. Arratia, Phys. Rev. Lett. **106**, 208101 (2011); B. Liu, T.R. Powers and K.S. Breuer, Proc. Natl. Acad. Sci. U.S.A. **108**, 19516 (2011); S.E. Spagnolie, B. Liu and T.R. Powers, Phys. Rev. Lett. **111**, 068101 (2013); B. Thomases and R.D. Guy, Phys. Rev. Lett. **113**, 098102 (2014).

[20] Y. Bozorgi and P.T. Underhill, J. Rheol. **57**, 511 (2013); Y. Bozorgi and P.T. Underhill, J. Non-Newton. Fluid Mech. **214**, 69 (2014).

[21] A.M. Ardekani and E. Gore, Phys. Rev. E **85**, 056309 (2012).

[22] E.J. Hemingway, A. Maitra, S. Banerjee, M.C. Marchetti, S. Ramaswamy, S.M. Fielding and M.E. Cates, Phys. Rev. Lett. **114**, 098302 (2015); E.J. Hemingway, M.E. Cates and S.M. Fielding, Phys. Rev. E **93**, 032702 (2016).

[23] Y. Amarouchene and H. Kellay, Phys. Rev. Lett. **89**, 104502 (2002).

[24] G. Boffetta, A. Celani and S. Musacchio, Phys. Rev. Lett. **91**, 034501 (2003).

[25] C.M. White and M.G. Mungal, Annu. Rev. Fluid Mech. **40**, 235 (2008); M.D. Graham, Phys. Fluids **26**, 101301 (2014).

[26] L. Xi, A. Celani and M.D. Graham, Phys. Rev. Lett. **21**, 218301 (2010).

[27] A.M. Ardekani, S. Dabiri and R.H. Rangel, J. Comput. Phys. **227**, 10094 (2008).

[28] Supplementary Material at. which includes Refs. [29-35].

[29] M. Rivera and X. L.Wu, Phys. Rev. Lett. **85**, 976 (2000).

[30] C.S. Peskin, Acta Numer. **11**, 479 (2002).

[31] S. Dabiri, J. Lu and G. Tryggvason, Phys. Fluid **25**, 102110 (2013); S. Dabiri and G. Tryggvason, Chem. Eng. Sci. **122**, 106 (2015); S. Dabiri, A. Doostmohammadi, M. Bayareh and A.M. Ardekani, Int. J. Multiph. Flow **69**, 8 (2015).

[32] R. Guénette and M. Fortin, J. Non-Newton. Fluid Mech. **60**, 27 (1995).

[33] R. Fattal and R. Kupferman, J. Non-Newton. Fluid Mech. **123**, 281 (2004).

[34] P.T. Underhill, J.P. Hernandez-Ortiz and M.D. Graham, Phys. Rev. Lett. **100**, 248101 (2008).

[35] T. Brotto, J.B. Caussin, E. Lauga and D. Bartolo, Phys. Rev. Lett. **110**, 038101 (2013).

[36] R.B. Bird, R.C. Armstrong, O. Hassager, *Dynamics of polymeric liquids. Vol. 1: Fluid mechanics* (Academic, New York, 1987).

[37] G. Li, A. Karimi, A.M. Ardekani, Rheol. Acta **53**, 911 (2014).

[38] P.C. Valente, C.B. da Silva and F.T. Pinho, J. Fluid Mech. **760**, 39 (2014).

[39] E. De Angelis, C.M. Casciola and R. Piva, Physica D **241**, 297 (2012).

[40] T. Ishikawa, N. Yoshida, H. Ueno, M. Wiedeman, Y. Imai and T. Yamaguchi, Phys. Rev. Lett. **107**, 028102 (2011).